International Journal of Microwave and Wireless Technologies

cambridge.org/mrf

An enhanced wideband tracking method for characteristic modes

Chao Huang, Chenjiang Guo, Xia Ma, Yi Yuan and Jun Ding

School of Electronics and Information, Northwestern Polytechnical University, Xi'an, China

Abstract

An enhanced wideband tracking method for characteristic modes (CMs) is investigated in this paper. The method consists of three stages, and its core tracking stage (CTS) is based on a classical eigenvector correlation-based algorithm. To decrease the tracking time and eliminate the crossing avoidance (CRA), we append a commonly used eigenvalue filter (EF) as the preprocessing stage and a novel postprocessing stage to the CTS. The proposed postprocessing stage can identify all CRA mode pairs by analyzing their trajectory and correlation characteristics. Subsequently, it can predict corresponding CRA frequencies and correct problematic qualities rapidly. Considering potential variations in eigenvector numbers at consecutive frequency samples caused by the EF, a new execution condition for the adaptive frequency adjustment in the CTS is introduced. Finally, CMs of a conductor plate and a fractal structure are investigated to demonstrate the performance of the proposed method, and the obtained results are discussed.

Research Paper

Cite this article: Huang C, Guo C, Ma X, Yuan Y, Ding J (2024). An enhanced wideband tracking method for characteristic modes. *International Journal of Microwave and Wireless Technologies* 1–11. https://doi.org/10.1017/S1759078724000229

Received: 20 November 2023
Revised: 17 January 2024
Accepted: 19 January 2024

Keywords:
characteristic modes; crossing avoidance; eigenvector correlation; mode tracking

Corresponding author: Chao Huang;
Email: huangchaoxidian@163.com

Introduction

The theory of characteristic mode (TCM), initially proposed by Garbacz *et al.* [1], has received much attention in recent years for its wide application in the electromagnetic field, particularly in antenna design [2, 3]. In the TCM, the radiating and scattering proprieties of arbitrary structures are intuitively obtained by solving a frequency domain generalized eigenvalue equation (GEE) defined by the method-of-moments (MoM) impedance matrix [4, 5]. The calculated eigenvalues and eigenvectors of characteristic modes (CMs) reflect their mode behaviors at each frequency. In practical applications, it is valuable for designers to have a clear understanding of how mode behaviors vary across a sequence of frequency samples. To capture the behavior changes of CMs across a wideband spectrum, the CM qualities, especially eigenvalues, should be organized in a certain order at all discrete frequencies [6]. Therefore, a method of modal tracking is needed.

Over the past decade, many efforts have been devoted to achieving modal tracking, predominantly relying on correlation-based algorithms with varied qualities, including eigenvalue [7], eigenvector [8], surface current [9], and far-field [10]. Among these, the eigenvector correlation-based algorithm (ECBA) is the most popular because it strikes a balance between accuracy and complexity. However, the initial ECBA, as presented in paper [8], suffers from errors such as mode swapping and crossing avoidance (CRA).

To address these challenges, several modified ECBAs have been proposed [11–13]. As a classical approach, the ECBA in paper [11] mitigates the mode swapping by introducing an arbitration stage. Its effective schemes involving the correlation matrix and adaptive tracking have been widely applied in subsequent studies. Moreover, in papers [12, 13], a strategy for eliminating the CRA is reported by exchanging eigenvalues and eigenvectors of CRA mode pairs. However, this strategy proves inadequate for correcting deformed modal currents in the problem areas because the CRA issue stems from coupling effects [14, 15], which cannot be fully resolved through simple exchanges. Besides tracking errors, the computational time of the tracking procedure is also significant for practical applications. In paper [16], the computational time of the ECBA is greatly reduced by limiting the number of eigenvectors to a fixed value. However, a fixed eigenvector number lacks robustness and is unsuitable for complex structures.

This paper proposes a multi-stage tracking method for wideband CM analysis. The classical ECBA in paper [11] is adopted as the core tracking stage (CTS) of the method. A preprocessing eigenvalue filter (EF) stage and a postprocessing stage are appended to the CTS to accelerate its tracking process and correct the CRA error. To demonstrate its effectiveness, CMs of a conductor plate and a fractal structure are examined using the proposed method. In comparison with other reported ECBA tracking methods, the proposed one introduces several novelties as follows:

(1) In the CTS: A new execution condition (NEC) for the adaptive frequency adjustment (AFA) is proposed to accommodate the mapping of two frequencies with different eigenvector numbers caused by the EF. The proposed condition enables obtaining complete eigenvalue traces with fewer additional frequency samples, thereby reducing the tracking time.
(2) In the postprocessing stage: A new strategy is proposed to identify all CRA mode pairs and rapidly predict their CRA frequencies with cubic spline interpolation (CSI). Additionally, a decoupled method rather than the simple quantity exchange is applied to eliminate the CRA issue, and the time of elimination is reduced by introducing a new stop criterion.

The organization of this paper is as follows. Section "Theoretical foundations" introduces the basic TCM and the classical ECBA, including its significant problems. In Section "Proposed tracking method", the proposed tracking method is presented in detail. A validation test of the method is performed by using two numerical examples in Section "Numerical example". Finally, a conclusion is drawn in Section "Conclusion".

Theoretical foundations

TCM

In the TCM, a field integral equation is discretized into a matrix form by the MoM in a frequency domain; consequently, its corresponding complex impedance matrix $\mathbf{Z}$ at any frequency f is generated to construct a GEE as [17]:

$$\mathbf{X}(f)\mathbf{J}_n(f) = \lambda_n(f)\mathbf{R}(f)\mathbf{J}_n(f) \tag{1}$$

where matrices $\mathbf{R}$ and $\mathbf{X}$ are real and imaginary parts of $\mathbf{Z}$, respectively. By solving equation (1), a set of eigenvalues λ_n and their corresponding eigenvectors $\mathbf{J}_n$ at f are obtained. The subscript n indicates the index of CMs.

As the most important CM quantity, λ_n is utilized to characterize the total stored field energy within a radiation or scattering problem. Since the value range $(-\infty, +\infty)$ of λ_n is too wide to observe, researchers often substitute it with the modal significance (MS) and the characteristic angle (CA) as:

$$\mathrm{MS}(f) = \frac{1}{|1 + j\lambda_n(f)|} \tag{2}$$

$$\mathrm{CA}(f) = 180^\circ - \tan^{-1}\lambda_n(f) \tag{3}$$

The MS and the CA are derived quantities of λ_n, and their variation ranges are $[0, 1]$ and $[90^\circ, 270^\circ]$, respectively. The case of $\lambda_n = 0$, which can be substituted with either MS $= 1$ or CA $= 180^\circ$, indicates that the associated CM is resonating.

In addition, the solved eigenvectors with distinct mode indexes satisfy the orthogonality conditions as:

$$\mathbf{J}_m^T(f)\mathbf{R}(f)\mathbf{J}_n(f) = 0 \tag{4}$$

$$\mathbf{J}_m^T(f)\mathbf{X}(f)\mathbf{J}_n(f) = 0 \tag{5}$$

where $m \neq n$. Also, they are normalized by the following equation:

$$\mathbf{J}_n^T(f)\mathbf{R}(f)\mathbf{J}_n(f) = 1 \tag{6}$$

The normalization is necessary in the CM tracking, ensuring the unit radiation power of CMs.

Table 1. Rule of thumb for interpreting PCC

Size of correlation	Interpretation
.90 to 1.00 (−.90 to −1.00)	Very high correlation
.70 to .90 (−.70 to −.90)	High correlation
.50 to .70 (−.50 to −.70)	Moderate correlation
.30 to .50 (−.30 to −.50)	Low correlation
.00 to .30 (.00 to −.30)	Negligible correlation

Wideband modal tracking problems

At the beginning of this subsection, we provide a brief overview of the classical ECBA in paper [11]. Its core tracking method is to construct a correlation matrix $\mathbf{C}$ for CMs at consecutive frequency samples f_i and f_{i+1} as

$$\mathbf{C} = [c_{mn}]_{N\times N} \tag{7}$$

where elements c_{mn} of $\mathbf{C}$ are the correlations between corresponding two sets of eigenvectors $\mathbf{J}_1(f_i) \sim \mathbf{J}_N(f_i)$ and $\mathbf{J}_1(f_{i+1}) \sim \mathbf{J}_N(f_{i+1})$ as

$$c_{mn} = |\rho(\mathbf{J}_m(f_i), \mathbf{J}_n(f_{i+1}))| \tag{8}$$

where operator $\rho(\cdot)$ is the Pearson correlation coefficient (PCC). If there are two vectors $\mathbf{X} = [x_1, x_2, \ldots, x_N]^T$ and $\mathbf{Y} = [y_1, y_2, \ldots, y_N]^T$, their PCC is calculated as

$$\rho(\mathbf{X}, \mathbf{Y}) = \frac{N\sum_{k=1}^{N} x_k y_k - \sum_{k=1}^{N} x_k \cdot \sum_{k=1}^{N} y_k}{\sqrt{N\sum_{k=1}^{N} x_k^2 - \left(\sum_{k=1}^{N} x_k\right)^2} \cdot \sqrt{N\sum_{k=1}^{N} y_k^2 - \left(\sum_{k=1}^{N} y_k\right)^2}} \tag{9}$$

Drawing on a widely acknowledged interpretation of PCC in Table 1 [18], judgements of the eigenvector mapping are delineated as follows: (1) If c_{mn} is the maximum element in the column n with a value above 0.9, then $\mathbf{J}_n(f_{i+1})$ is mapped to $\mathbf{J}_m(f_i)$; (2) If multiple eigenvectors at f_{i+1} are mapped to a particular eigenvector at f_i, only the one with maximum $|\rho|$ is selected. The first judgement ensures that mapped eigenvectors exhibit very high correlations, while the second one aims to alleviate correlation ambiguities.

Moreover, a classical adaptive strategy for frequency adjustment is also presented in paper [11]. Specifically, if there are unmapped eigenvectors at f_i or f_{i+1}, a new sample is added between f_i and f_{i+1}. This strategy has been widely used in other reported tracking methods [9, 12], which can further improve the accuracy. The traces of tracked CMs can be determined by iteratively applying the above procedure across all sampling frequencies. Although the above classical ECBA is effective and significantly mitigates the mode swapping, it still suffers from the following problems that need to be addressed:

CRA

The CRA, also referred to as "mode degeneracy" in other literature [7, 12], is exemplified in Fig. 1. The CRA may occur at a specific frequency when a pair of modes possess approaching eigenvalues. This phenomenon is well documented in the field of quantum physics, which is elucidated as a perturbation for the Hermitian matrix [19]. In electromagnetics, this perturbation is recognized as a coupling effect, indicating that the occurrence of the CRA is

https://doi.org/10.1017/S1759078724000229 Published online by Cambridge University Press

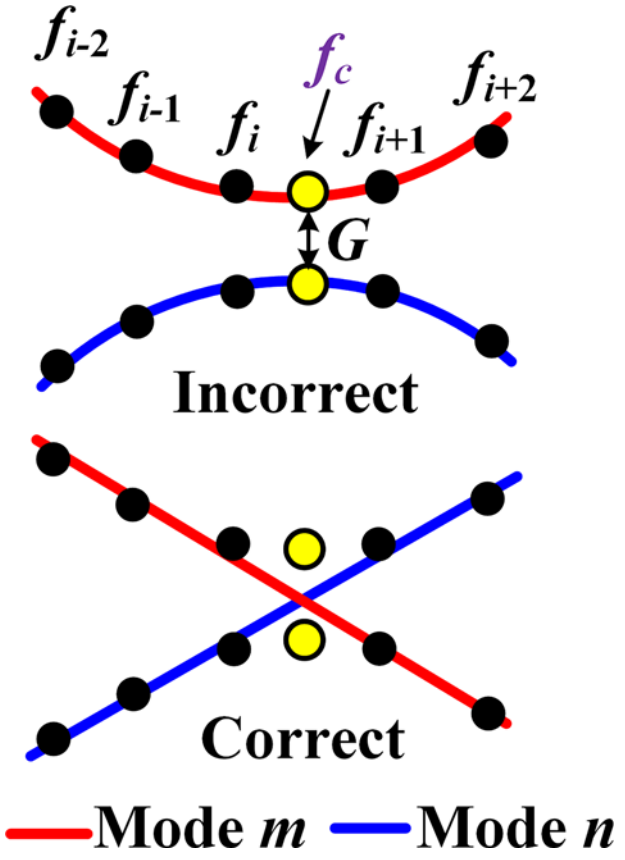

Figure 1. Sketches of CRA (incorrect) and normal intersection (correct). Dots and solid lines represent the raw unsorted data and the tracking traces, respectively.

more likely to be found in an energy-coupled system [20]. The CRA frequency f_c featuring the strongest coupling energy between the investigated mode pair exhibits the closest eigenvalue difference $\Delta\lambda_{mn}$, defined as

$$f_c = \arg\min\{|\Delta\lambda_{mn}(f)|\} \tag{10}$$

where

$$\Delta\lambda_{mn}(f) = \lambda_m(f) - \lambda_n(f) \tag{11}$$

The closest eigenvalue difference is termed as G, given by

$$G = \min\{|\Delta\lambda_{mn}(f)|\} \tag{12}$$

At frequency f_c, eigenvalue curves are split; the surface current of CM is strongly deformed; the current distribution can transition from one situation to another, which is why the CRA should be corrected. Three significant challenges must be tackled to effectively eliminate the CRA: recognizing all CRA mode pairs, determining their CRA frequencies, and correcting eigenvalues and eigenvectors.

High computational time

The TCM is a frequency-domain modal analysis method. For a wideband CM analysis, the eigenvalues and the eigenvectors are solved and mapped iteratively across numerous sampling frequencies. The computational complexity associated with the ECBA at each sampling frequency is of $O(K \times N^2)$ [16], where N is the number of basis functions in the MoM, and K is the number of eigenvectors. Therefore, with a fixed tracking algorithm, an increase in the number of sampling frequencies results in higher computational time, which is particularly evident in the wideband CM tracking.

Proposed tracking method

This paper introduces an optimized tracking method to address the problems outlined in Section "Theoretical foundations". The procedure of the proposed method consists of multiple stages, namely, the preprocessing EF stage, the CTS, and the postprocessing stage, with a flowchart provided in Fig. 2. The roles of these three stages can be briefly outlined as (1) EF stage: remove insignificant eigenvalues and their corresponding eigenvectors; (2) CTS: obtain preliminary tracking results; and (3) postprocessing stage: eliminate CRA errors. Detailed explanations of each section are provided in the subsequent subsections.

Preprocessing EF stage

After presetting the tracking range (from f_{start} to f_{end}) and the initial frequency step (STP), the proposed procedure starts by solving the GEE at two consecutive frequency samples (f_i and f_{i+1}). Subsequently, their corresponding eigenvalues $\lambda_{1\sim\max}$ and eigenvectors $\mathbf{J}_{1\sim\max}$ can be obtained. The acquired data then proceed to the preprocessing EF stage. In this stage, a filter is introduced to remove insignificant CMs by constraining the range of $|\lambda_n|$ to be less than 100. Consequently, the number of mapped eigenvectors can be greatly decreased. Similar strategies and the threshold of 100 have been commonly adopted in other literature [8, 9], aiming to alleviate the computational complexity.

CTS

After the EF, the data are transmitted to the CTS, which is a modified version of the classical ECBA discussed in Section "Theoretical foundations". Compared with the classical ECBA, our modification focuses on adjusting the execution condition for the AFA. Due to the utilization of the EF, the number of eigenvectors in the CTS may not be equal at f_i and f_{i+1}, i.e., $K(f_i) \neq K(f_{i+1})$, and their matrix $\mathbf{C}$ may not be a square matrix. When this happens, according to the classical ECBA, a new frequency sample should be added between f_i and f_{i+1} to avoid the presence of unmapped eigenvectors at either f_i or f_{i+1}. However, such processing is inappropriate and time-consuming since the issue of different K persists in the tracking range no matter how many samples are added.

We illustrate our adaptive strategy for $K(f_i) < K(f_{i+1})$ and $K(f_i) > K(f_{i+1})$ through two special cases (Case I and Case II) depicted in Fig. 3(a) and (b), respectively. In Case I, no unmapped eigenvectors exist at f_i; the remaining $\mathbf{J}_4(f_{i+1})$ indicates the emergence of a new CM index $\mathrm{M_a}$ at f_{i+1}. Conversely, in Case II, all the eigenvectors at f_{i+1} are mapped; the remaining $\mathbf{J}_4(f_i)$ indicates the disappearance of the previous CM index $\mathrm{M_b}$. In these cases, we only need to consider the appropriateness of the start frequency f_{i+1} for $\mathrm{M_a}$ and the end frequency f_i for $\mathrm{M_b}$. For a complete CM trace, its $|\lambda_n|$ should feature a large value at the start and end frequencies. Therefore, if $|\lambda_4(f_{i+1})|$ of $\mathrm{M_a}$ or $|\lambda_4(f_i)|$ of $\mathrm{M_b}$ is smaller than a certain threshold, then the AFA is executed to ensure the integrity of tracking results. After numerous experiments, we set the threshold to 10 in this paper.

(b) Case II: $K(f_i) > K(f_{i+1})$.

Based on the above analysis, we propose an NEC for the AFA, involving three comparison statements as

https://doi.org/10.1017/S1759078724000229 Published online by Cambridge University Press

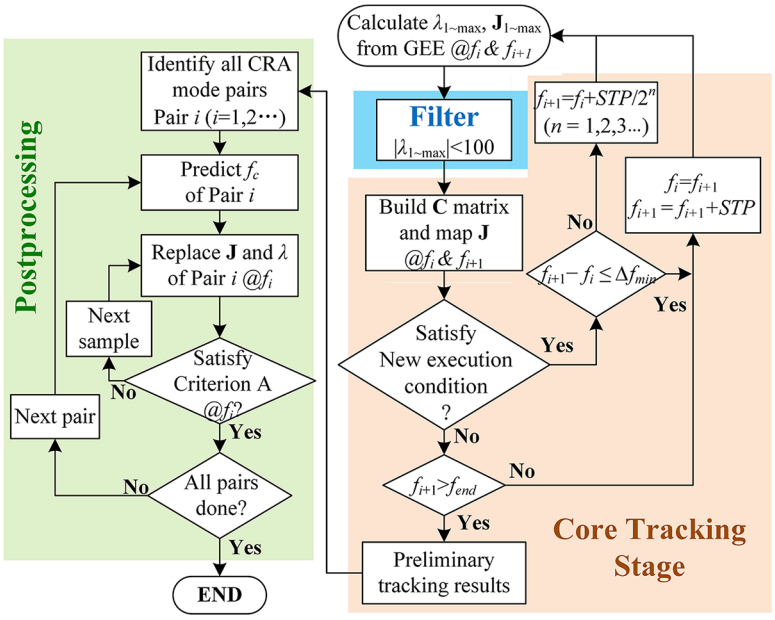

Figure 2. Flowchart of the proposed CM tracking procedure.

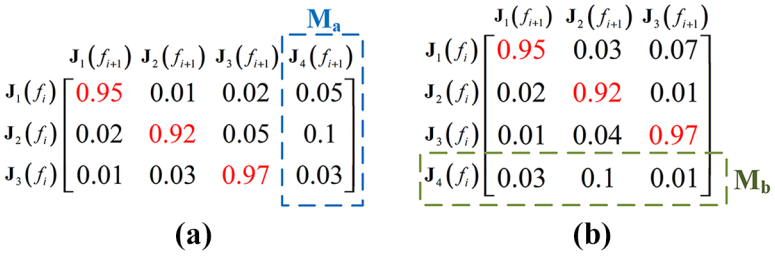

Figure 3. **C** matrixes of two special cases. (a) Case I: $K(f_i) < K(f_{i+1})$.

(1) If $K(f_i) = K(f_{i+1})$, the AFA executes when unmapped eigenvectors exist;
(2) If $K(f_i) < K(f_{i+1})$, the AFA executes when unmapped eigenvectors exist at f_i, and $|\lambda_n|$ of emerging CMs is smaller than 10;
(3) If $K(f_i) > K(f_{i+1})$, the AFA executes when unmapped eigenvectors exist at f_{i+1}, and $|\lambda_n|$ of disappearing CMs is smaller than 10;

Among them, the first statement is identical to the one in the classical EBCA. The second and third statements enable us to obtain complete traces of emerging and disappearing CMs while also reducing the probability of executing the AFA when $K(f_i) \neq K(f_{i+1})$. This approach is time-saving and enhances the overall efficiency.

In the proposed AFA, the interval between f_i and f_{i+1} (Δf) will be repeatedly divided into subintervals, and the process will stop when the NEC is not satisfied, or Δf is smaller than the preset threshold $\Delta f_{\min}$. The CTS commences at f_{start} and concludes when the mapping at f_{end} is complete.

Postprocessing

Finally, the preliminary tracking data acquired through the CTS flows to the postprocessing stage, designed to tackle the CRA issue. The fundamental concept of this stage is to integrate the coupled-mode theory into the TCM. The theory and the implementation of the CRA elimination are presented in the following subsections.

Theory of CRA elimination

The theory employed for CRA elimination is grounded in coupled-mode theory, as documented in paper [21]. If M_1 (with $\mathbf{J}_1$ and λ_1) and M_2 (with $\mathbf{J}_2$ and λ_2) are a pair of CRA modes, their CRA issues at any frequency f can be resolved by replacing their eigenvalues and eigenvectors with the qualities in an auxiliary system, defined as

$$\mathbf{X}(f)\mathbf{J}_a(f) = \lambda_a(f)\mathbf{R}(f)\mathbf{J}_a(f) + \mathbf{H}\mathbf{J}_b(f) \tag{13}$$

$$\mathbf{X}(f)\mathbf{J}_b(f) = \lambda_b(f)\mathbf{R}(f)\mathbf{J}_b(f) + \mathbf{H}\mathbf{J}_a(f) \tag{14}$$

where $\mathbf{J}_a$ and $\mathbf{J}_b$ are two auxiliary vectors with orthonormality, and $\mathbf{H}$ is a coupling matrix. Notably, the values of λ_a and λ_b are set to be equal at f_c for the normal intersection. Equations (13) and (14) establish a new system that effectively integrates the coupled-mode theory with the TCM. Subsequently, the eigenvectors of M_1 and M_2 are decomposed into the linear combination of $\mathbf{J}_a$ and $\mathbf{J}_b$, guided by their orthonormality, expressed as

$$\mathbf{J}_1(f) = \cos\alpha(f)\mathbf{J}_a(f) + \sin\alpha(f)\mathbf{J}_b(f) \tag{15}$$

$$\mathbf{J}_2(f) = -\sin\alpha(f)\mathbf{J}_a(f) + \cos\alpha(f)\mathbf{J}_b(f) \tag{16}$$

https://doi.org/10.1017/S1759078724000229 Published online by Cambridge University Press

Consequently, a relationship between $\lambda_{1,2}$ and $\lambda_{a,b}$ is obtained as

$$\lambda_{1,2}(f) = \frac{\lambda_a(f) + \lambda_b(f)}{2} \pm \sqrt{\left(\frac{\lambda_a(f) - \lambda_b(f)}{2}\right)^2 + \left(\frac{G}{2}\right)^2} \tag{17}$$

Moreover, the expression of the coefficient α is derived as

$$\alpha(f) = \tan^{-1}\frac{2(\lambda_1(f) - \lambda_a(f))}{G} \tag{18}$$

The expressions of eigenvalues and α in paper [21] are slightly different from the proposed ones, stemming from variations in the definition of decomposition coefficients and G.

By inverting equation (17) and ensuring the consistency of eigenvalue traces, we derive the expressions of independent λ_a and λ_b as

$$\lambda_a(f) = \begin{cases} \frac{\lambda_1(f)+\lambda_2(f)}{2} + \sqrt{\left(\frac{\lambda_1(f)-\lambda_2(f)}{2}\right)^2 - \left(\frac{G}{2}\right)^2} & f < f_c \\ \frac{\lambda_1(f)+\lambda_2(f)}{2} - \sqrt{\left(\frac{\lambda_1(f)-\lambda_2(f)}{2}\right)^2 - \left(\frac{G}{2}\right)^2} & f > f_c \end{cases} \tag{19}$$

$$\lambda_b(f) = \begin{cases} \frac{\lambda_1(f)+\lambda_2(f)}{2} - \sqrt{\left(\frac{\lambda_1(f)-\lambda_2(f)}{2}\right)^2 - \left(\frac{G}{2}\right)^2} & f < f_c \\ \frac{\lambda_1(f)+\lambda_2(f)}{2} + \sqrt{\left(\frac{\lambda_1(f)-\lambda_2(f)}{2}\right)^2 - \left(\frac{G}{2}\right)^2} & f > f_c \end{cases} \tag{20}$$

In addition, $\mathbf{J}_a$ and $\mathbf{J}_b$ can be calculated by inverting equations (15) and (16) as

$$\mathbf{J}_a(f) = \cos\alpha(f)\,\mathbf{J}_1(f) - \sin\alpha(f)\,\mathbf{J}_2(f) \tag{21}$$

$$\mathbf{J}_b(f) = \sin\alpha(f)\,\mathbf{J}_1(f) + \cos\alpha(f)\,\mathbf{J}_2(f) \tag{22}$$

For M_1 and M_2, the CRA can be eliminated by replacing the quantities λ_1, λ_2, $\mathbf{J}_1$, and $\mathbf{J}_2$ with their respective auxiliary counterparts λ_a, λ_b, $\mathbf{J}_a$, and $\mathbf{J}_b$.

Implementation of CRA elimination

In this subsection, we discuss the detailed information of the postprocessing stage. This stage is based on the CRA elimination theory mentioned in the previous subsection and comprises three key steps.

The first step is to identify all CRA mode pairs within the tracking range. The central challenge in this step is to recognize the CRA phenomenon effectively. It is observed that a CRA is likely to occur between a pair of CMs when their mode behaviors satisfy the following criteria at three consecutive frequency samples (f_{i-1}, f_i, and f_{i+1}) as

$$\begin{cases} \frac{\Delta\lambda_{mn}(f_{i-1})}{\Delta\lambda_{mn}(f_i)} > 1 \\ \frac{\Delta\lambda_{mn}(f_{i+1})}{\Delta\lambda_{mn}(f_i)} > 1 \end{cases} \tag{23}$$

$$|\rho(\mathbf{J}_m(f_i), \mathbf{J}_n(f_i))| > 0.3 \tag{24}$$

The first criterion involves evaluating $\Delta\lambda_{mn}$ between two modes. As depicted in Fig. 1, when f_c is within the range from f_{i-1} to f_{i+1},

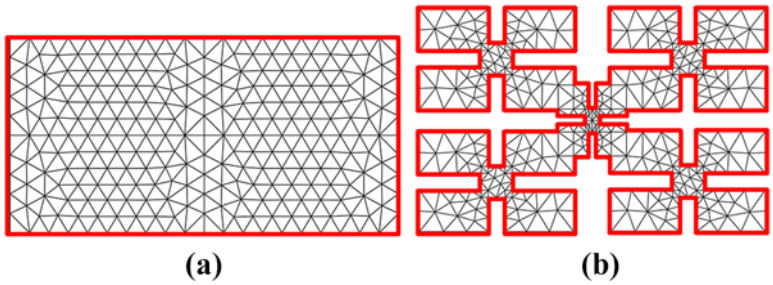

Figure 4. Geometry and mesh views of the demonstration examples. (a) Rectangular conductor plate. (b) Fractal structure.

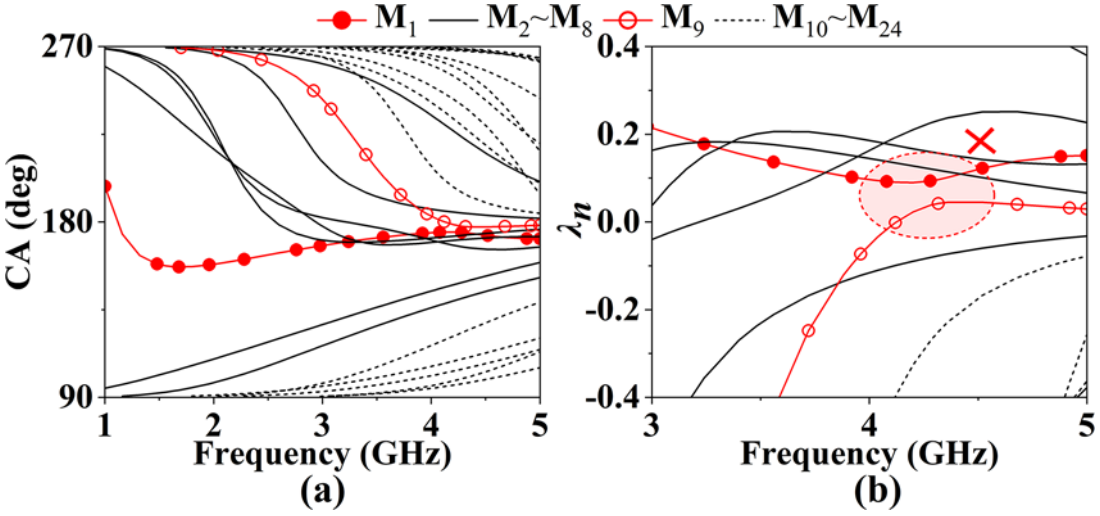

Figure 5. Tracking results of the conductor plate without the postprocessing. (a) Entire-band view in CAs. (b) Zoomed-in view in eigenvalues.

https://doi.org/10.1017/S1759078724000229 Published online by Cambridge University Press

$\Delta\lambda_{mn}$ exhibits a fixed variation pattern at f_{i-1}, f_i, and f_{i+1}, i.e., small at f_i and large at f_{i-1} and f_{i+1}. In addition, the signs of $\Delta\lambda_{mn}$ at f_{i-1}, f_i, and f_{i+1} are identical. The above characteristics of $\Delta\lambda_{mn}$ can be captured in equation (23). However, mode pairs without CRA issues may also exhibit these features of $\Delta\lambda_{mn}$. To address this potential issue, we propose an additional criterion in equation (24) to determine whether the recognized CRA mode pair has a nonnegligible correlation. Consequently, all CRA mode pairs can be identified by iteratively estimating mode behaviors for any two modes across all sampling frequencies. Moreover, the frequency range in which the CRA occurs for each mode pair can also be available.

The second step involves determining the CRA frequency f_c and, consequently, the value of G for a CRA mode pair (Pair i). With knowledge of the frequency range of f_c, adding more frequency samples in that range is conventional to find a frequency closer to f_c [14]. However, since these newly added samples are unsorted, a significant amount of tracking time will be spent by using this strategy. This paper employs CSI to predict f_c due to its ability to generate smooth curves with a consecutive second derivative [22]. For instance, if we have determined Modes m and n in Fig. 1 as a pair of CRA modes with $f_{i-1} < f_c < f_{i+1}$ through the first step, then CSI is performed to obtain the piecewise trace functions for the two CMs in the intervals of $f_{i-1} < f < f_i$ and $f_i < f < f_{i+1}$. Specifically, for Mode n, its piecewise trace functions are calculated using the eigenvalue data of the three knots f_{i-1}, f_i, and f_{i+1}, and two slope values, m_1 and m_2, at f_{i-1} and f_{i+1} are also considered as

$$m_1 = \frac{\lambda_n(f_{i-1}) - \lambda_n(f_{i-2})}{f_{i-1} - f_{i-2}} \tag{25}$$

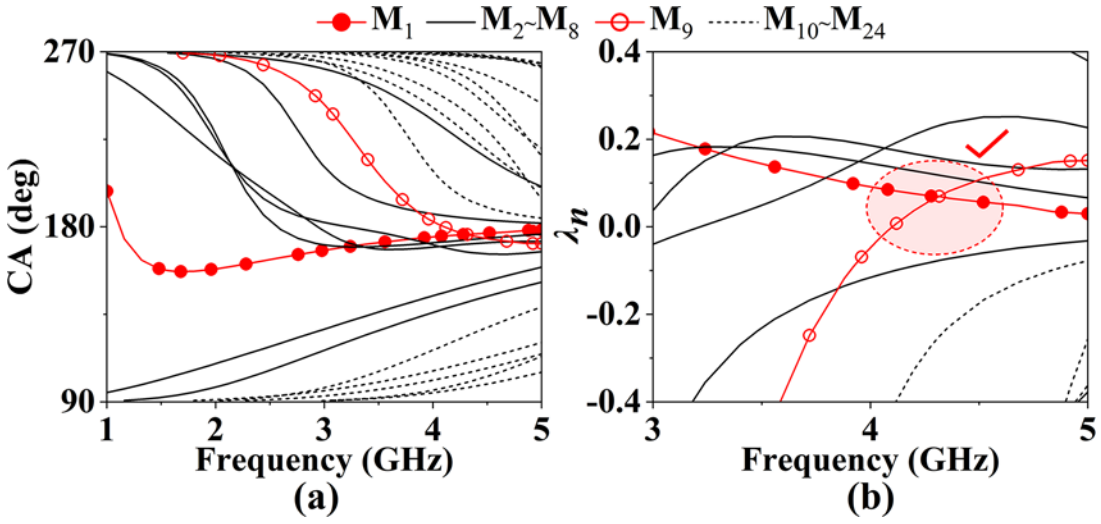

Figure 6. Tracking results of the conductor plate with the postprocessing. (a) Entire-band view in CAs. (b) Zoomed-in view in eigenvalues.

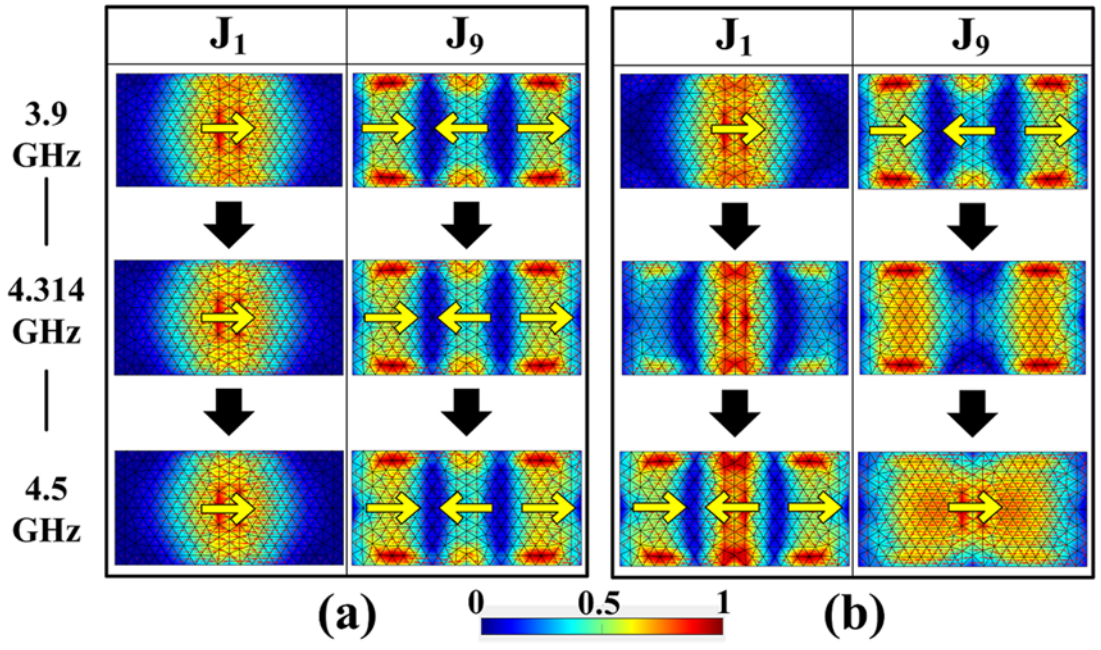

Figure 7. Normalized modal current distributions of M_1 and M_9. (a) With the postprocessing. (b) Without the postprocessing.

https://doi.org/10.1017/S1759078724000229 Published online by Cambridge University Press

$$m_2 = \frac{\lambda_n(f_{i+2}) - \lambda_n(f_{i+1})}{f_{i+2} - f_{i+1}} \tag{26}$$

where f_{i-2} and f_{i+2} are the previous and the subsequent frequencies of f_{i-1} and f_{i+1}, respectively. Consequently, the piecewise trace functions of the two CRA modes can be determined, and a frequency with the smallest $|\Delta\lambda_{mn}|$ can be found easily. The obtained frequency is the predicted f_c, and its corresponding $|\Delta\lambda_{mn}|$ is considered as G. This strategy is time-saving because no extra unsorted frequency samples are introduced. The prediction error is also acceptable due to the consistency of eigenvalue traces.

According to the theory of CRA elimination, the CRA issue can be effectively addressed by replacing the original CM quantities

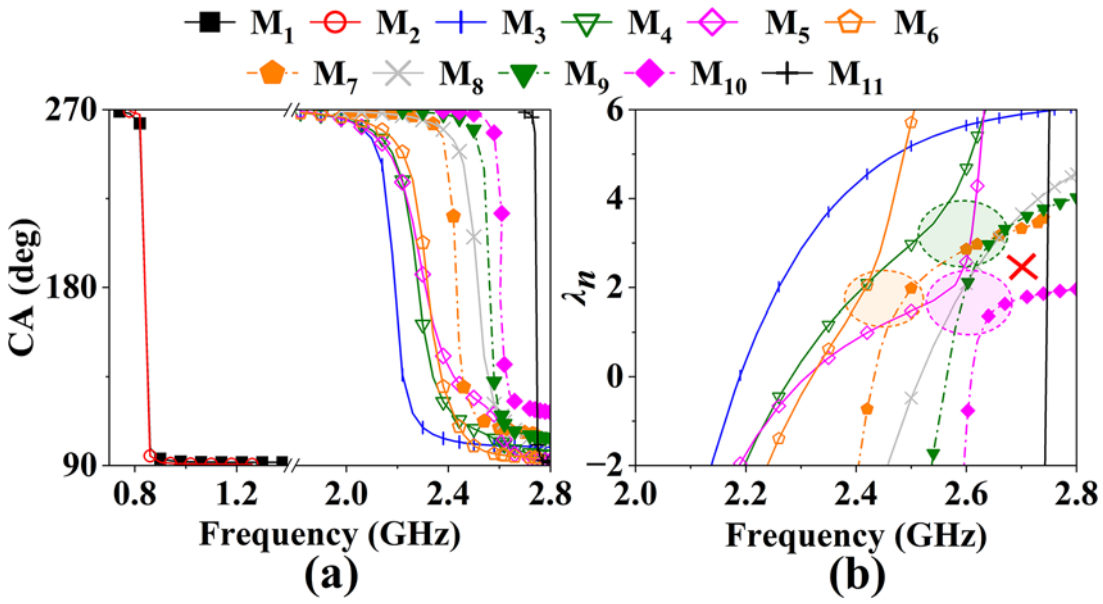

Figure 8. Tracking results of the fractal structure without the postprocessing. (a) Entire-band view in CAs. (b) Zoomed-in view in eigenvalues.

Table 2. Detailed information for Pairs 1–3

Mode pairs	Range f_c	Predicted f_c	G	Replaced range	Replaced number/proportion
Pair 1	2.58–2.62 GHz	2.603 GHz	1.335	2.42–2.8 GHz	22/33.3%
Pair 2	2.42–2.5 GHz	2.443 GHz	1.104	2.34–2.64 GHz	13/19.6%
Pair 3	2.6–2.64 GHz	2.610 GHz	1.570	2.46–2.8 GHz	20/30.3%

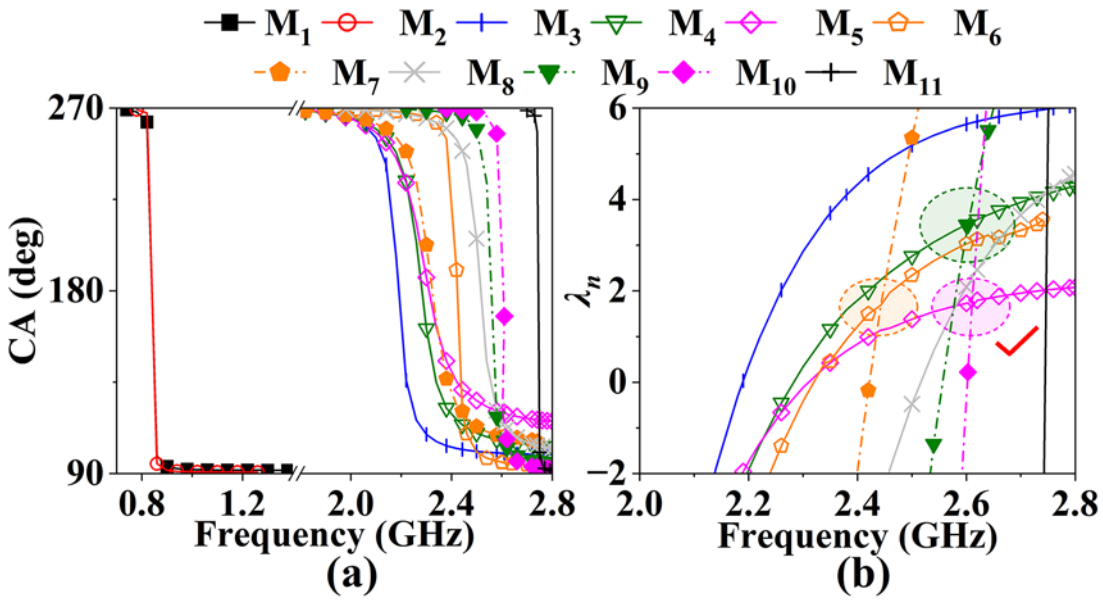

Figure 9. Tracking results of the fractal structure with the postprocessing. (a) Entire-band view in CAs. (b) Zoomed-in view in eigenvalues.

https://doi.org/10.1017/S1759078724000229 Published online by Cambridge University Press

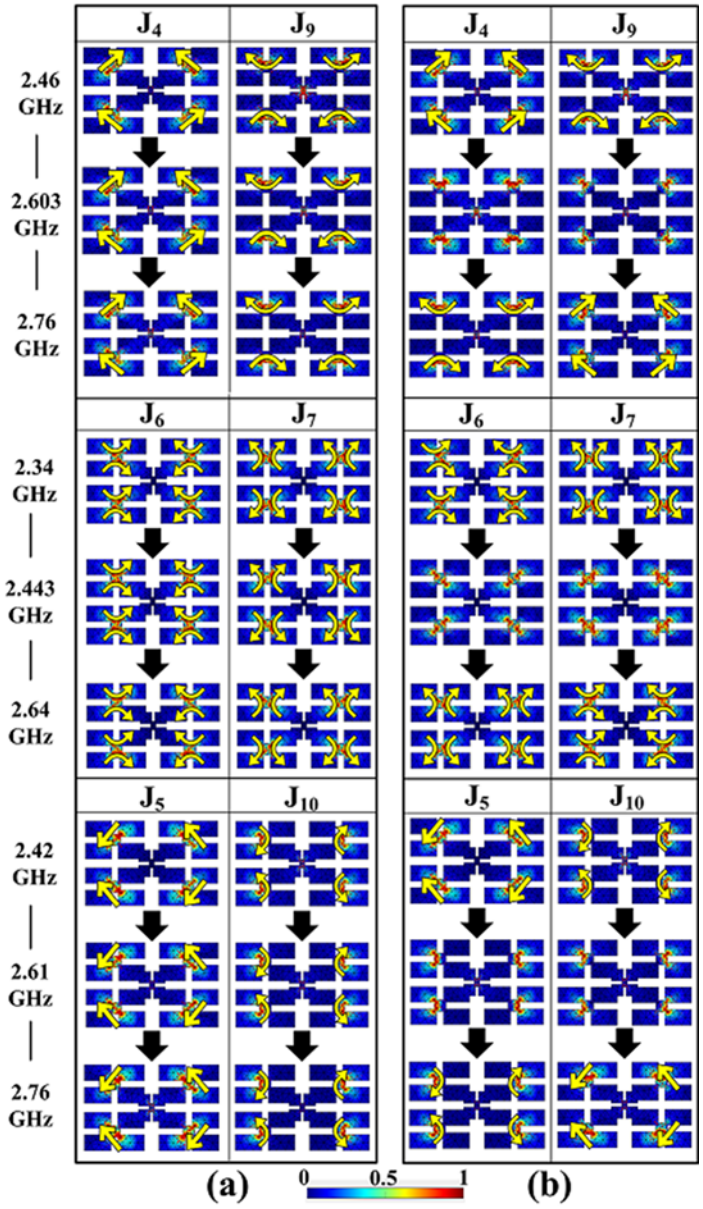

Figure 10. Normalized modal current distributions of the three CRA mode pairs. (a) With the postprocessing. (b) Without the postprocessing.

Table 3. Computational time of four different tracking methods (unit: s)

	i	ii	iii	iv
Conductor plate	6634.72	179.63	42.52	43.76
Fractal structure	7327.34	92.92	61.79	64.78

i: Classical ECBA [11], ii: Classical ECBA + EF [9], iii: Classical ECBA + EF + NEC, iv: Classical ECBA + EF + NEC + Postprocessing (Proposed).

with their corresponding auxiliary counterparts. Therefore, in the third step, auxiliary quantities λ_a, λ_b, $\mathbf{J}_a$, and $\mathbf{J}_b$ of Pair i are calculated at a certain frequency f_i by equations (19–22) at first. Then, they replace the original eigenvalues and eigenvectors at f_i. While other studies perform the replacement across all frequencies in the tracking range [14, 21], in this paper, the replacement is made only at a few frequencies. The decision is supported by the observation that as the investigated frequency moves away from f_c, CMs in Pair i exhibit a weakly coupled effect, causing their eigenvectors and eigenvalues to resemble auxiliary counterparts. Therefore, performing the replacement at all frequencies is deemed unnecessary in most cases, as it would consume more computational time. In this paper, the replacement starts at f_c and proceeds to the higher and lower frequencies. The replacement ends when the original eigenvectors, such as $\mathbf{J}_1$ and $\mathbf{J}_2$, exhibit a very high correlation with their auxiliary vectors, i.e., $|\rho(\mathbf{J}_1(f_i), \mathbf{J}_a(f_i))| > 0.9$ or $|\rho(\mathbf{J}_2(f_i), \mathbf{J}_b(f_i))| > 0.9$ (Criterion A). Finally, the entire procedure of the proposed CM tracking method is complete when the replacement of the last CRA mode pair is done.

Numerical example

In this section, the applicability of the proposed method is validated by tracking CMs of two classical structures. Both structures share common configurations, with $\Delta f_{\min}$ set to 10 MHz and the CSI accuracy set to 1 MHz. All numerical simulations are performed using MATLAB R2022b, employing double precision on

https://doi.org/10.1017/S1759078724000229 Published online by Cambridge University Press

a desktop computer equipped with Intel Core i5-10600KF processor and 32 GB of RAM within a Windows 10 Professional 64-bit environment.

Example 1: Rectangular conductor plate

As shown in Fig. 4(a), the first example is a rectangular conductor plate with dimensions of 60×120 mm^2, which has been widely used in other studies [9, 13]. The plate was discretized with 456 triangular elements and subjected to the MoM analysis utilizing 654 Rao–Wilton–Glisson (RWG) basis functions from 1 to 5 GHz with *STP* of 160 MHz. After applying the EF, there were 50 pairs of consecutive frequency samples with unequal *K*, and none of them needed to execute the AFA by using the NEC. Consequently, 42 frequency samples were utilized in this tracking example. Following the CTS, 24 valid CMs (M_1–M_{24}) were acquired, and their CA result without the postprocessing is depicted in Fig. 5(a). The result presents no mode sweeping, and all CMs seem to be tracked correctly. However, using the first step of the postprocessing, an unnoticeable CRA error between M_1 and M_9 in the range from 4.2 to 4.36 GHz was found, showing more obviously in Fig. 5(b).

Then, for M_1 and M_9, CSI was performed with the eigenvalues at 4.2, 4.28, and 4.36 GHz, along with corresponding endpoint slopes. Consequently, f_c for M_1 and M_9 was determined as 4.314 GHz, with a *G* value of 0.027. The replacement of the original eigenvalues and eigenvectors of M_1 and M_9 with corresponding auxiliary quantities started at 4.314 GHz and stopped at 3.88 and 4.68 GHz, accounting for only 24.5% of the total frequency samples. The final tracking CA results are presented in Fig. 6(a), revealing a normal trace intersection of M_1 and M_9, as observed in Fig. 6(b). Additionally, as shown in Fig. 7(a), there is no erroneous modal current exchange at f_c for M_1 and M_9 after the postprocessing, and their current distribution at f_c is undeformed. For comparison, the original modal current distributions of M_1 and M_9 are provided in Fig. 7(b).

Example 2: Fractal structure

As shown in Fig. 4(b), the second example features a fractal structure with dimensions identical to those in papers [8, 12]. Compared with the plate, the fractal structure presents a more challenging tracking scenario due to an increased number of CRA. The MoM analysis for the fractal structure utilized 700 RWG basis functions over the range from 0.7 to 2.8 GHz with *STP* of 40 MHz. Following the application of the proposed EF, there were 17 pairs of consecutive frequency samples with unequal *K*. Among these, only two pairs needed to execute the AFA using the proposed NEC. Consequently, 66 frequency samples were utilized in this tracking example. After the CTS, 11 valid CMs (M_1–M_{11}) were obtained, and their CA result without the postprocessing is depicted in Fig. 8(a). Utilizing the first step of the postprocessing, three CRA mode pairs were identified, i.e., Pair 1 (M_4 and M_9), Pair 2 (M_6 and M_7), and Pair 3 (M_5 and M_{10}), as highlighted in Fig. 8(b).

Like the first example, CRA issues within Pairs 1–3 were resolved by predicting their CRA frequencies f_c using CSI, calculating their corresponding auxiliary quantities, and replacing their original eigenvalues and eigenvectors. The predicted and replacement information for Pairs 1–3 is detailed in Table 2. The final tracking CA results are presented in Fig. 9(a). As illustrated in Fig. 9(b), CMs in Pairs 1–3 exhibit correct intersections after the postprocessing, highlighting the capability of the proposed method to correct multiple CRA mode pairs simultaneously. Moreover, the original incorrect modal current distributions of CMs in Pairs 1–3, as shown in Fig. 10(a), were rectified to a consistent and undeformed state after the postprocessing, as demonstrated in Fig. 10(b).

In addition to its enhanced accuracy, the proposed method provides benefits in terms of reduced tracking time and decreased sensitivity to the initial frequency step size. The computational time for several different tracking methods applied to the two examples is recorded in Table 3. Notably, the time for solving GEE was considered. A comparison of methods i–iii reveals a significant reduction in computational time by incorporating the EF, and an additional reduction is observed with the implementation of the NEC. Moreover, the time difference between methods iii and iv is less than 4.83%, indicating that the extra time cost by the postprocessing is acceptable.

To assess the sensitivity to the frequency step, the plate was tested with *STP* ranging from 10 to 320 MHz, and the fractal

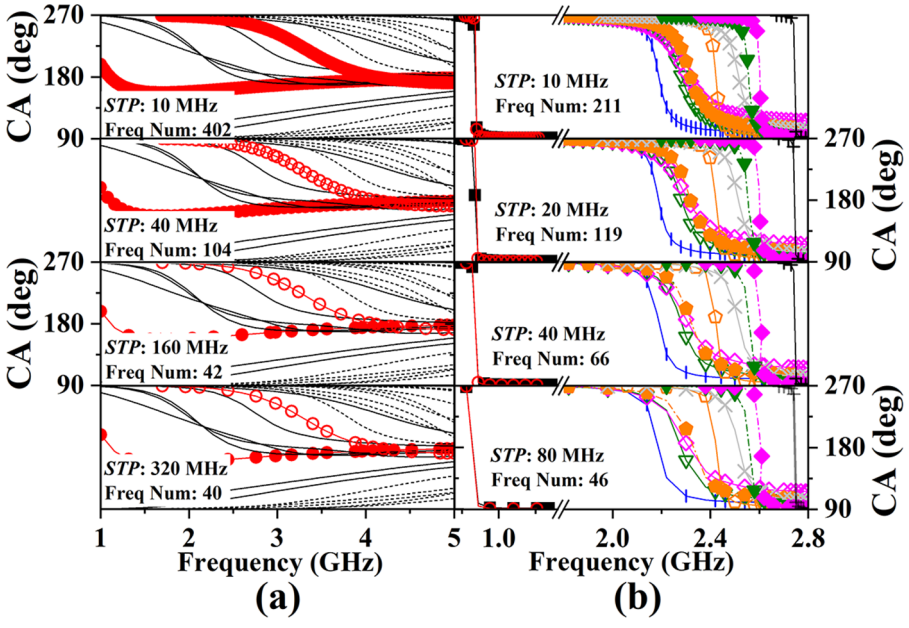

Figure 11. Tracking CA results with different *STP*. (a) Conductor plate. (b) Fractal structure.

https://doi.org/10.1017/S1759078724000229 Published online by Cambridge University Press

structure was tested with *STP* ranging from 10 to 80 MHz. Their corresponding tracking CA results, along with information on the number of frequency samples, are depicted in Fig. 11. The proposed method here exhibits lower sensitivity to *STP* variations. As *STP* increases exponentially, there is no proportional decrease in the number of frequency samples. This behavior can be attributed to the proposed AFA, which ensures that the frequency samples crucial for tracking accuracy are not omitted. Therefore, a larger *STP* only results in less smooth tracking results rather than introducing errors.

Conclusion

In this paper, an enhanced ECBA-based tracking method for wideband CMs is developed. Our proposed method comprises distinct stages where the CTS is rooted in a classical ECBA. The efficiency and accuracy of the CTS are significantly improved through the incorporation of a preprocessing EF stage and a postprocessing stage. Additionally, we proposed an NEC for the AFA in the CTS to better accommodate the introduction of the EF. The proposed EF and NEC collectively contribute to a substantial reduction in the tracking time, while the proposed postprocessing stage identifies and eliminates all CRA mode pairs rapidly. For demonstration, this method has been applied to investigate a conductor plate and a fractal structure, and satisfying tracking performance has been obtained.

Compared with the existing ECBA-based approaches, our proposed tracking method offers several advantages: (1) it not only eliminates CRA eigenvalue traces but also corrects corresponding deformed eigenvectors; (2) it requires fewer frequency samples and less computational time; and (3) it is less sensitive to the initial frequency step. As a result, the proposed method is a good candidate for CM tracking, especially in wideband applications.

Competing interests. We declare that all authors have no conflicts of interest.

References

1. **Garbacz R and Turpin R** (1971) A generalized expansion for radiated and scattered fields. *IEEE Transactions on Antennas and Propagation* **19**, 348–358.
2. **Rajanna PK, Rudramuni K and Kandasamy K** (2020) Characteristic mode-based compact circularly polarized metasurface antenna for in-band RCS reduction. *International Journal of Microwave and Wireless Technologies* **12**, 131–137.
3. **Jayant S, Srivastava G and Kumar S** (2023) Pattern diversity and isolation enhancement of UWB MIMO antenna based on characteristic modes for mobile terminals. *International Journal of Microwave and Wireless Technologies* **15**, 793–804.
4. **Harrington RF and Mautz JR** (1971) Computation of characteristic modes for conducting bodies. *IEEE Transactions on Antennas and Propagation* **19**, 629–639.
5. **Harrington RF and Mautz JR** (1971) Theory of characteristic modes for conducting bodies. *IEEE Transactions on Antennas and Propagation* **19**, 622–628.
6. **Gustafsson M, Jelinek L, Schab K and Capek M** (2022) Unified theory of characteristic modes—Part I: Fundamentals. *IEEE Transactions on Antennas and Propagation* **70**, 11801–11813.
7. **Akrou L and Silva HJAD** (2019) Enhanced modal tracking for characteristic modes. *IEEE Transactions on Antennas and Propagation* **67**, 356–360.
8. **Capek M, Hazdra P, Hamouz P and Eichler J** (2011) A method for tracking characteristic numbers and vectors. *Progress in Electromagnetics Research B* **33**, 115–134.
9. **Safin E and Manteuffel D** (2016) Advanced eigenvalue tracking of characteristic modes. *IEEE Transactions on Antennas and Propagation* **64**, 2628–2636.
10. **Miers Z and Lau BK** (2015) Wideband characteristic mode tracking utilizing far-field patterns. *IEEE Antennas and Wireless Propagation Letters* **14**, 1658–1661.
11. **Raines BD and Rojas RG** (2012) Wideband characteristic mode tracking. *IEEE Transactions on Antennas and Propagation* **60**, 3537–3541.
12. **Chen JX, Pan YM and Su DG** (2021) An advanced eigenvector-correlation-based tracking method for characteristic modes. *IEEE Transactions on Antennas and Propagation* **69**, 2751–2758.
13. **Shavakand MY, Shokouh JA and Dashti H** (2023) A fast multi-structural tracking method for characteristic modes with the ability to identify and amend errors. *IET Microwaves, Antennas and Propagation* **17**, 62–74.
14. **Sun ZF, Li WW and Liu QH** (2022) Judgment of mode crossing avoidance in characteristic mode analysis. *Journal of Electromagnetic Waves and Applications* **36**, 2549–2566.
15. **Schab KR and Bernhard JT** (2017) A group theory rule for predicting eigenvalue crossings in characteristic mode analyses. *IEEE Antennas and Wireless Propagation Letters* **16**, 944–947.
16. **Li WW, Zhu JB, Xu B and Zeng ZJ** (2018) Fast implementation of characteristic mode tracking. *IET Microwaves, Antennas and Propagation* **12**, 2179–2183.
17. **Chen YK and Wang CF** (2015) *Characteristics Modes: Theory and Applications in Antenna Engineering*. Hoboken, New Jersey: John Wiley & Sons Press.
18. **Hinkle DE, Wiersma W and Jurs SG** (2003) *Applied Statistics for the Behavioural Sciences*, 5th edn. Boston: Houghton Mifflin Press.
19. **Neumann JV and Wigner E** (2000) *On the Behaviour of Eigenvalues in Adiabatic Processes*. Singapore: Word Scientific Press.
20. **Haus H and Huang W** (1991) Coupled-mode theory. *Proceedings of the IEEE* **79**, 1505–1518.
21. **Schab KR, Outwater JM, Young MW and Bernhard JT** (2016) Eigenvalue crossing avoidance in characteristic modes. *IEEE Transactions on Antennas and Propagation* **64**, 2617–2627.
22. **Burden RL, Faires JD and Burden AM** (2015) *Numerical Analysis*, 10th edn. Boston: Cengage Learning Press.

Chao Huang was born in Xi'an, Shaanxi, China, in March 1994. He received the bachelor's and master's degrees from the School of Electronic Engineering, Xidian University, Xi'an, China, in 2016 and 2019, respectively. He is currently pursuing the Ph.D. degree in the School of Electronics and Information, Northwestern Polytechnical University, Xi'an, China. His current research interests include characteristic mode theory and its applications in high performance or multifunctional antennas.

Chenjiang Guo was born in February 1963. He received the B.S. degree, M.S. degree, and Ph.D. degree from the Northwestern Polytechnical University, Xi'an, China, in 1984, 1987, and 2007, respectively. In 1987, he joined Northwestern Polytechnical University, China, as an Assistant Professor, where he is a Full Professor. His current research interests include electromagnetic metasurface, antenna theory and design, microwave circuit design, and electromagnetic compatibility.

https://doi.org/10.1017/S1759078724000229 Published online by Cambridge University Press

Xia Ma was born in Guyuan, Ningxia, China, in April 1995. She received the B.S. degree in electronic information science and technology and M.S. degree in information and communication engineering from Xi'an University of Science and Technology, Xi'an, Shaanxi, in 2019 and 2022, respectively. She is currently pursuing the Ph.D. degree in electronic information from the Northwestern Polytechnical University, Xi'an, China. Her research interests include frequency-selective rasorber, RCS reduction metasurface, and reconfigurable metasurface.

Yi Yuan was born in Nanyang, Henan, China, in 1997. He received the B.S. degree in electronics and information engineering from Zhengzhou University, Zhengzhou, China, in 2019. He is currently pursuing the Ph.D. degree in electronics science and technology from the Northwestern Polytechnical University, Xi'an, China. His current research interests include metasurface, method of moment, and antenna design.

Jun Ding was born in 1964. She received the B.S. degree, M.S. degree, and Ph.D. degree from the Northwestern Polytechnical University, Xi'an, China, in 1986, 1989, and 2005, respectively. In 1989, she joined Northwestern Polytechnical University, China, as an Assistant Professor, where she is a Full Professor. Her current research interests include electromagnetic calculation, antenna theory and design, microwave circuit design, electromagnetic stealth technology, and electromagnetic metamaterial design.

https://doi.org/10.1017/S1759078724000229 Published online by Cambridge University Press